13th International Symposium on Particle Image Velocimetry – ISPIV 2019
Munich, Germany, July 22-24, 2019

Research of drag reduction mechanism of micro riblets of supercritical airfoil

Zhan Huang*, Hongwei Wang, Minglei Yuan

China Academy of Aerospace Aerodynamics, Beijing, China

*xfd_huangzh@sina.com

Abstract

For the conventional civil aviation aircraft, skin friction accounts for about a large proportion of the total resistance. Understanding the generation mechanism of high frictional resistance of turbulent boundary layer is the basis of reducing the frictional resistance of turbulent boundary layer. In recent years, with the development of experiments and turbulence simulation technology, it has been recognized that the surface of ribbed grooves with appropriate shape, scale and layout has obvious effect of restraining turbulence frictional resistance. In this paper, the research of drag reduction mechanism of micro riblets of supercritical airfoil was carried out in transonic wind tunnel test. TSP technology was used to determine the flow pattern of airfoil surface, and PIV, TOMOPIV were used to verify the effect of drag reduction of micro riblets. PIV and fluorescence oil film were also measured for one flat plate model, the effect of drag reduction of micro riblets was also verified.

1 Introduction

For conventional civil aviation aircraft, the skin friction accounts for about 50% of the total resistance, drag reduction is not only directly related to the performance of civil aviation aircraft, but also indirectly affect the flight cost and environmental protection. On most areas of the surface of a civil aircraft, the flow is in turbulent state, so it is of great significance to study turbulent boundary layer drag reduction, which has been listed as one of the key aviation technologies in the 21st century by NASA. Research on drag reduction could date back to the 1930s, but until the mid-1960s, much of the work focused on reducing surface roughness, with the implicit assumption that smooth surfaces have the least drag. However, experiments with different flow conditions have shown that smooth surfaces are not the best for reducing drag as Darcy experiment described. In the 1970s, NASA langley research center found that the longitudinal micro riblets grooved surface could effectively reduce the skin friction[1], breaking through the traditional mode of thinking that the smoother the surface, the less the resistance. After that, the longitudinal micro riblets became the research focus of turbulence drag reduction technology.

In the early stage, researches on drag reduction generally focused on the direct measurement of wall resistance by means of force balance. With the development of research, researchers have paid more and more attention to the study of the internal flow structure and related laws of turbulence boundary layer on micro riblets grooved surface. Through micro riblets of different sizes installed on smooth plate, Wang jinjun confirmed that the micro riblets grooved surface not only can delay boundary layer transition[2], but also has the characteristics of drag reduction in turbulent boundary layer, and can change the turbulence characteristics in the near wall region [2][3][4], and drag reduction is related to the decrease of dimensionless strip spacing in the near-wall region[5]. The results of experiments conducted by Choi[5] and Orchard in the low-speed boundary layer wind

tunnel at Nottingham university showed that, in the nonlinear phase of transition, the growth rate of momentum thickness decreases along with the decrease of the turbulence intensity above the micro riblets, and indicated that the micro riblets has an obvious delay effect on transition from laminar boundary layer to turbulence. However, until now, there are still different opinions on whether the turbulivity and burst frequency of turbulent boundary layer above micro riblets increase, decrease or remain unchanged[6][7][8][9]. By analyzing the flow visualization results, Wang jinjun found that the low speed streaks appear to be flat and linear. This means that the stream-wise riblets limit the flow motion in the spanwise direction, and the flow stability is enhanced[10]. S.J.Lee[11] Visualized the flow structure of NACA 0012 airfoil coated by micro riblets film by smoke wire method and found that micro riblets make the smoke line thinner and separated with small lateral spacing. This indicates that the spanwise movement is suppressed.

In the systematic study including the shape, size and layout of the micro riblets, Walsh and his collaborators[12][13][14][15] at NASA's langley research center carried out a number of experiments on micro riblets of different shapes(including triangle, rectangle, V shape, semicircle, etc.), and found that triangular shaped micro riblets groove surfaces appear to be optimum performance. When the dimensionless size of height h+ and spacing s+ are less than 25 and 30, micro riblets have characteristics of drag reduction. The optimum dimensionless size is h+=s+=15, the drag can be reduced by 8%. Chamorro et al[16] carried out experiments on micro riblets films of different sizes and shapes and found that drag reduction for the micro riblet is dependent on the height and spacing and geometric profile, and v-shaped groove has the best drag reduction effect. Wilkinson and Lazos first developed thin-element-riblets, namely quadrilateral micro riblets surfaces with different aspect ratio, and conducted a lot of experiments in low-speed wind tunnels[17]. Drag reduction was found to be roughly proportional to the height and inversely proportional to the spacing. Maximum drag reduction occurred on the micro riblets surfaces of high aspect ratio, it was equivalent to 8% drag reduction of the symmetric v-shaped micro riblets and similar to Walsh's conclusion. Choi[18] and Walsh believed that the micro riblets with drag reduction effect must have sharp peak ridge, and the spacing between the riblets is related to the spacing between low-speed strips. It is generally agreed that when the dimensionless spacing and dimensionless height of micro riblets are less than 30, the micro riblets surface has a drag reduction effect.

In this paper, the research of drag reduction mechanism of micro riblets of supercritical airfoil was carried out in transonic wind tunnel test. PSP/TSP technology was used to determine the flow pattern of airfoil surface, and PIV, TOMOPIV were used to verify the effect of drag reduction of micro riblets. PIV and fluorescence oil film were also measured for one flat plate model, the effect of drag reduction of micro riblets was also verified.

2 Design and processing of micro riblets film

The parameters of micro riblets groove are generally calculated by the following formula,

$$s^+ = \frac{su^*}{\nu} \quad h^+ = \frac{hu^*}{\nu} \quad u^* = \sqrt{\tau_w / \rho} \tag{1}$$

Where, s is the width, s^+ is the dimensionless width, h is the peak height of the peak, h^+ is the dimensionless height, u^* is the wall friction velocity, τ_w is the wall friction shear stress. Correspondingly, the larger the local Reynolds number is, the smaller the absolute height and width of the ribbed will be under the same dimensionless height and width. The micro riblets film is producted by the hot pressing process of the hub. PVC film adhesive material is used as the production material, which is composed of surface PVC film, intermediate rubber layer and release paper. In this experiment, two kinds of micro riblets films named micro riblets film 1# and micro riblets film 2# were used for experiment. The height of the micro riblets film 1# was 22 microns, and the spacing between micro riblets was 27 microns. The height of the micro riblets film 2# was 30 microns, and the spacing between micro riblets was 40 microns.

Figure 1 Dimension parameter sketch and morphology detection of micro riblets

Table 1 Dimensionless scale of micro riblets film 1#

Mach	Supercritical airfoil		Flat plate	
	h+	s+	h+	s+
0.6	10.89378635	13.36964688	10.16426207	12.47432163
0.7	12.27798652	15.068438	11.45576649	14.05934978

Table 2 Dimensionless scale of micro riblets film 1#

Mach	Supercritical airfoil		Flat plate	
	h+	s+	h+	s+
0.6	14.8551632	19.80688427	13.86035736	18.48047648
0.7	16.74270889	22.32361185	15.62149976	20.82866634

3 PIV test and results of airfoil and plate

Supercritical airfoil model and plate model were used in PIV test. The purpose of airfoil model test was to verify and evaluate the effectiveness of micro riblets in inhibiting turbulent friction resistance by measuring the change of flow structure and velocity field after the micro riblets film had been adopted on the surface of airfoil model. In the plate model test, the influence of the micro riblets film on the velocity field can be measured more directly and effectively, and the PIV measurement accuracy can be verified by the measurement results of velocity field above the plate. The airfoil model used in the test is oat15-a model, with side window bracing specially designed to support the model. The flow field above the airfoil model can be detected by CCD camera from the side through the observation window. The layout of PIV test is shown in Figure 2. Under the condition of 0° Angle of attack and Mach 0.6 and 0.7, PIV test was conducted for comparative measurement for the distribution of the velocity field of the symmetrical section in the middle section of model coated by smooth film or micro riblets film, as shown in Figure 3. Figure 4 shows the PIV test layout of micro riblets film drag reduction of flat plate model. The length of the flat plate model is 600mm, width is 500mm, and tripping wire is attached at 5cm from the leading edge.

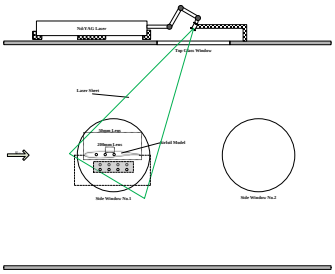

Figure 2 PIV test Layout of airfoil

Figure 3 Layout scheme of smooth film and riblets film

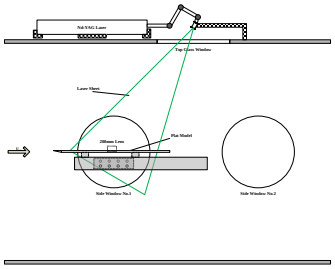

Figure 4 PIV test layout of flat plate

Experimental wind tunnel is an intermittent sub-transonic wind tunnel, and the total temperature

will change obviously during operation of wind tunnel. The total temperature will affect the velocity value of the flow field. It may be inaccurate to analyze the drag reduction effect of micro riblets film simply from the PIV velocity field results. Therefore, combined with PIV velocity field results and total temperature condition of inlet, the Mach number distribution of the flow field was calculated according to adiabatic hypothesis, and the drag reduction effect of micro riblets film was verified by comparing Mach number distribution.

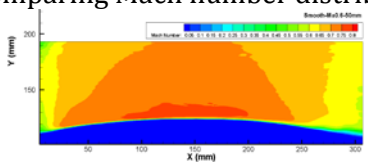

Figure 5 Distribution of Mach number(Ma0.6, f=50mm, smooth film)

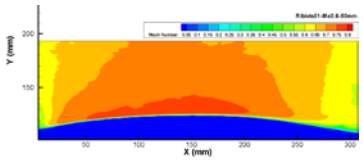

Figure 6 Distribution of Mach number(Ma0.6, f=50mm, 1# micro riblets film)

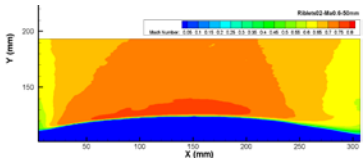

Figure 7 Distribution of Mach number(Ma0.6, f=50mm, 2# micro riblets film)

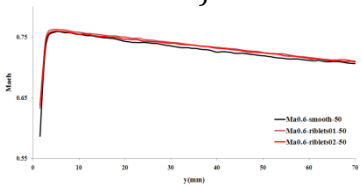

Figure 8 Comparision of Mach number Distribution(Ma0.6, f=50mm)

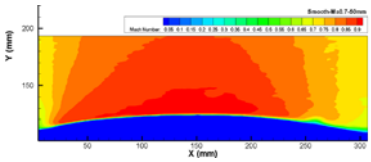

Figure 9 Distribution of Mach number(Ma0.7, f=50mm, smooth film)

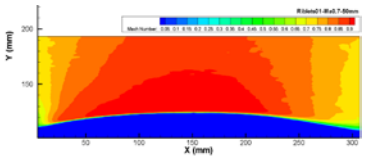

Figure 10 Distribution of Mach number(Ma0.7, f=50mm, 1# micro riblets film)

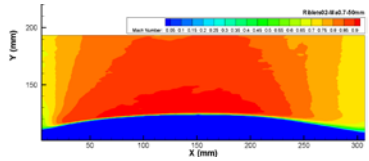

Figure 11 Distribution of Mach number(Ma0.7, f=50mm, 2# micro riblets film)

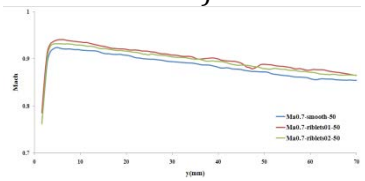

Figure 12 Comparision of Mach number Distribution(Ma0.7, f=50mm)

First, a 50mm lens was used to capture and observe the flow field in a large area. By comparing the Figure 5, Figure 6, Figure 7 and Figure 8, it can be seen that for smooth film, the Mach number distribution is the smallest, while for 1 # micro riblets film and 2 # micro riblets film, the Mach number distribution is relatively close and higher than that for smooth films. Near the wall, the Mach number distribution of 1# micro riblets film is slightly smaller than that of 2# micro riblets film, far from the wall, the Mach number distribution of 1# micro riblets film is slightly larger than that of 2# micro riblets film. By comparing the Figure 9 and Figure 10, Figure 11 and Figure 12, it can be seen also that for smooth film, the Mach number distribution is the smallest, while for 1 # micro riblets film and 2 # micro riblets film, the Mach number distribution is relatively close and significantly higher than that for smooth films, the Mach number distribution of 1 # micro riblets film is slightly higher than that of 2# micro riblets film.

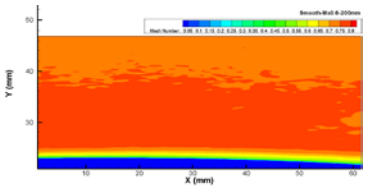

Figure 13 Distribution of Mach number(Ma0.6, f=200mm, smooth film)

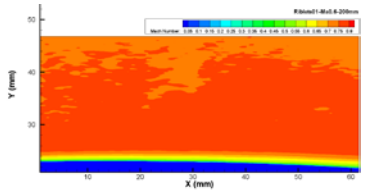

Figure 14 Distribution of Mach number(Ma0.6, f=200mm, 1# micro riblets film)

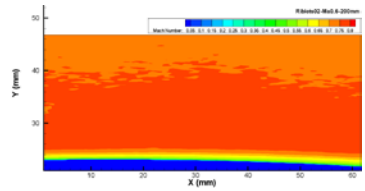

Figure 15 Distribution of Mach number(Ma0.6, f=200mm, 2# micro riblets film)

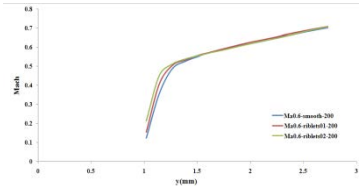

Figure 16 Comparision of Mach number Distribution(Ma0.6, f=200mm)

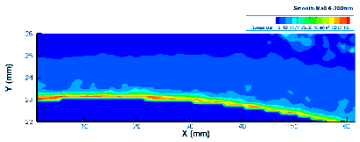

Figure 17 Distribution of fluctuation velocity(Ma0.6, f=200mm, smooth film)

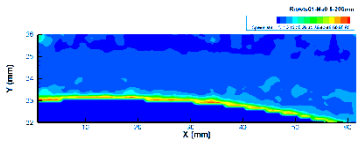

Figure 18 Distribution of fluctuation velocity(Ma0.6, f=200mm, 1# micro riblets film)

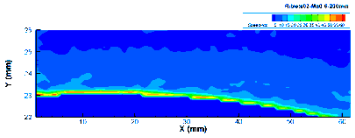

Figure 19 Distribution of fluctuation velocity(Ma0.6, f=200mm, 2# micro riblets film)

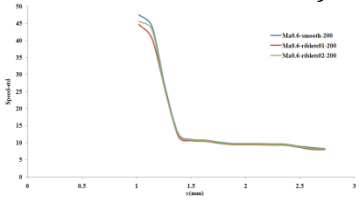

Figure 20 Comparision of fluctuation velocity Distribution(Ma0.6, f=200mm)

Further, a 200mm lens was used to capture and observe the flow field in a small area. Figure 13, Figure 14, Figure 15 and Figure 16 show the distribution and comparison of Mach number of flow field over three kinds of films of airfoil (Ma0.6, f=200mm). Figure 17, Figure 18, Figure 19 and Figure 20 show the distribution and comparison of fluctuation velocity of flow field over three kinds of films of airfoil (Ma0.6, f=200mm). It can be seen that the Mach number distribution for the smooth film is the smallest, especially in the boundary layer, the Mach number distribution of 1# micro riblets film is slightly smaller than that of 2# micro riblets film, and is significantly higher than that of the smooth film. At the same time, the fluctuation velocity of flow field in the boundary layer of smooth film is higher than that of 1# micro riblets film and 2# micro riblets film.

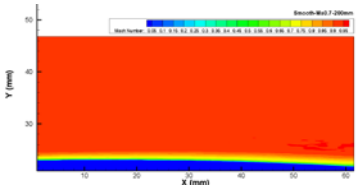

Figure 21 Distribution of Mach number(Ma0.6, f=200mm, smooth film)

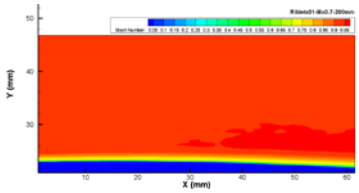

Figure 22 Distribution of Mach number(Ma0.7, f=200mm, 1# micro riblets film)

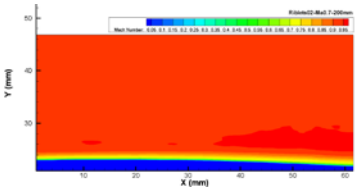

Figure 23 Distribution of Mach number(Ma0.7, f=200mm, 2# micro riblets film)

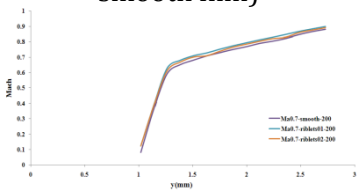

Figure 24 Comparision of Mach number Distribution(Ma0.7, f=200mm)

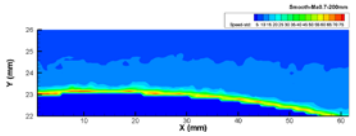

Figure 25 Distribution of fluctuation velocity(Ma0.7, f=200mm, smooth film)

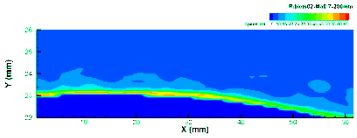

Figure 26 Distribution of fluctuation velocity(Ma0.7, f=200mm, 1# micro riblets film)

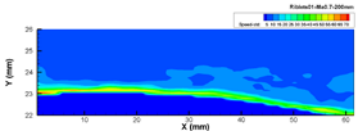

Figure 27 Distribution of fluctuation velocity(Ma0.7, f=200mm, 2# micro riblets film)

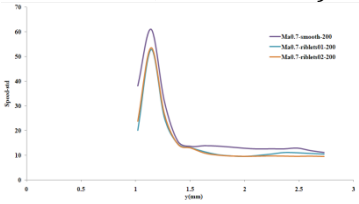

Figure 28 Comparision of fluctuation velocity Distribution(Ma0.7, f=200mm)

Figure 21, Figure 22, Figure 23 and Figure 24 show the distribution and comparison of Mach number of flow field over three thin films of airfoils (Ma0.7, f=200mm). Figure 25, Figure 26, Figure 27 and Figure 28 show the distribution and comparison of fluctuation velocity of flow field over three thin films of airfoils (Ma0.7, f=200mm). It can be seen that the Mach number distribution for the smooth film is the smallest, especially in the boundary layer, while for 1 # micro riblets film and 2 # micro riblets film, the Mach number distribution is very close, almost coincident, and obviously higher than that of smooth film. At the same time, the fluctuation velocity of flow field in the boundary layer of smooth film is higher than that of 1# micro riblets film and 2# micro riblets film.

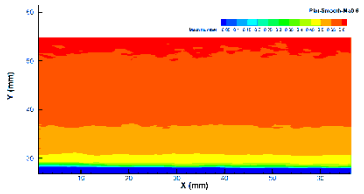

Figure 29 Distribution of Mach number(Ma0.6, f=200mm, smooth film, plate)

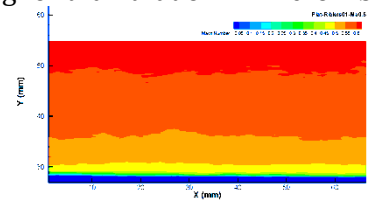

Figure 30 Distribution of Mach number(Ma0.6, f=200mm, 1# micro riblets film, plate)

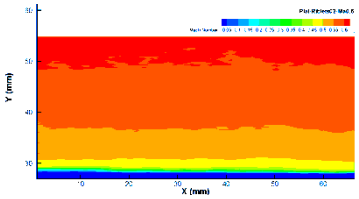

Figure 31 Distribution of Mach number(Ma0.6, f=200mm, 2# micro riblets film, plate)

Figure 29, Figure 30 and Figure 31 show the Mach number distribution of flow field over three kinds of films of plate (Ma0.7, f=200mm). Through comparison, it can be seen that the presence of micro riblets make the high-speed region of flow field move down and the boundary layer thickness decreases. On the other hand, the Mach number measured above the plate shows that the Mach number measured in the main flow area is very close to 0.6. Since the plate model does not cause any acceleration effect on the incoming flow, it indicates that the measurement accuracy of PIV system can meet the experimental requirements.

4 PSP/TSP tests and results of airfoil

Pressure sensitive paint (PSP) and the temperature sensitive paint (TSP) is new kinds of optical sensors based on luminescent oxygen quenching and light emitting thermal quenching, which use optical properties to measure temperature distribution and pressure distribution on the surface of model. Namely, special pressure/temperature sensitive paints are covered on the surface of the model. The paints can emit fluorescence when it is irradiated by a certain wavelength of light. The pressure and temperature distribution can be calculated by measuring the emission intensity field. PSP and TSP technologies provide noncontact optical thermal measurements and pressure measurements with high spatial resolution for surface pressure and temperature measurements of complex aerodynamic models at low cost. Pressure and temperature distribution of supercritical airfoil OTA151 surface were measured by pressure sensitive paint and temperature sensitive paint (Ma=0.6, 0.7). The basic configuration of PSP and TSP test system mainly includes excitation light source, camera, coated model, filter and data acquisition and processing. The test camera is PCO.1600 camera with a depth of 14bit and a resolution of 1200×1600 pixels. A 35mm focus lens is installed on the camera, and under the premise of ensuring that the collected images are not exposed, the aperture is set to the maximum to receive the fluorescence from the pressure/temperature sensitive paint while the wind tunnel is running.

The purpose of PSP test is to check whether the basic surface pressure distribution on the airfoil conforms to the theoretical data, and to check the influence of gap flow and tripping wire on the pressure distribution. Several blowing tests were conducted to verify the surface pressure distribution results measured by PSP under Ma=0.6 and Ma=0.7 conditions. The incoming flow direction is from the bottom to the top, and the surface pressure changes tend to be flat. On the surface of the model, the pressure decreases after the high pressure area at the leading edge, and gradually increases after the low pressure area, while the high pressure area appears at the trailing edge. With the increase of Mach number, the overall pressure decreases, but the pressure distribution tends to be consistent.

Reproducibility test were carried out to verify the measurement accuracy of PSP technology, as shown in Figure 34, result of reproducibility test of PSP(Ma=0.7). Considering the stability of wind tunnel flow field, the measurement uncertainty of PSP was within 5%. Figure 35 is result of reproducibility test of PSP(Ma=0.7), it is found that the overall pressure on the upper surface decreases somewhat due to the tripping wire pasted on the leading edge, and the pressure distribution tends to be flat.

By observing the pressure distribution cloud diagram under different Mach Numbers and different working conditions, it was found that the pressure in the left gap was slightly reduced, but the comparison of the force measurement results showed that the influence on the lift and drag coefficients was small and could be ignored.

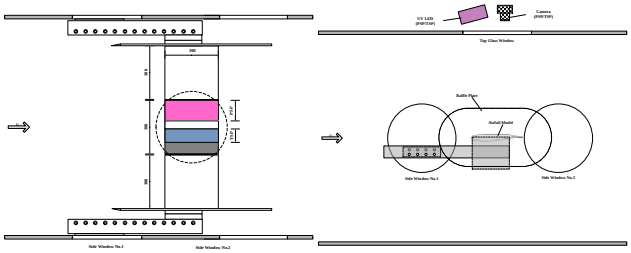

Figure 32 PSP/TSP test layout of airfoil

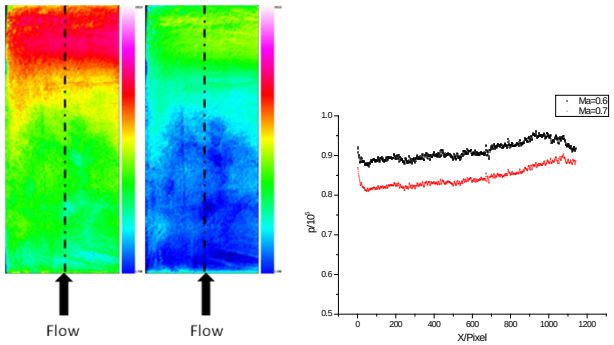

Cloud picture of surface pressure (Ma=0.6, 0.7)

Comparison of pressure distribution in center line

Figure 33 Comparison results of surface pressure distribution(Ma=0.6, 0.7)

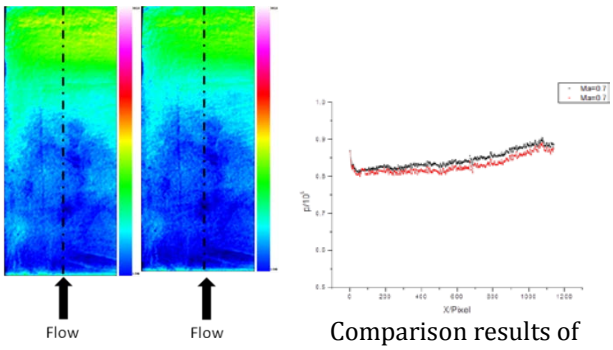

Cloud picture of surface pressure (Ma=0.7)

Comparison results of pressure distribution in center line

Figure 34 Result of reproducibility test of PSP(Ma=0.7)

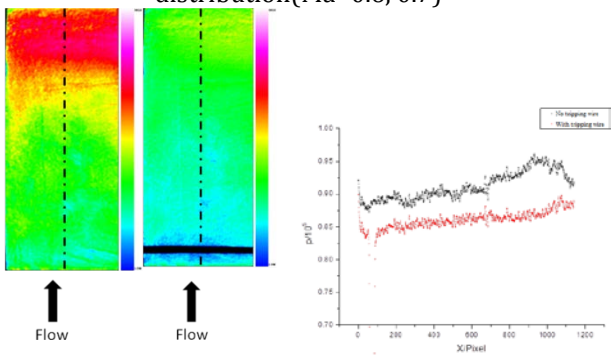

Cloud picture of surface pressure (Ma=0.6)

Comparison of pressure distribution in center line

Figure 35 Influence of tripping wire on surface pressure distribution(Ma=0.6, PSP)

Since the purpose of TSP test is to measure the position of transition region and ensure that the flow of airfoil surface develop into turbulence by means of manual forced transition, and thus distinguish the effect of micro riblets drag reduction under turbulence conditions, so it is not necessary to calculate the actual temperature value, but only the relative temperature distribution.

Before transition, the heat exchange coefficient of laminar flow area is small, while after transition, the heat exchange coefficient of turbulence area is large. When there is a temperature difference between the airflow and the model, due to the difference in heat exchange rate between the laminar flow area and the turbulence area, there is a temperature difference between the laminar flow area and the turbulence area. The whole airfoil is heated to a uniform temperature by spotlight heating for a long time before blowing. In the process of blowing, the heat transfer coefficients of laminar flow area and turbulence flow area are different. On the surface of high-temperature airfoil, the heat exchange coefficient of turbulence area is large, and more heat(Calories) is taken away under the cold flow condition of the incoming flow, so the temperature difference in the turbulence area is larger than that in the laminar flow area.

After the above analysis, the heat loss is different due to different heat exchange coefficients in laminar flow area and turbulence area. The heat exchange coefficient in the turbulence area is large, while the heat exchange coefficient in the laminar flow area is relatively small. Therefore, after the blowing process, the turbulence area will lose more heat, and the temperature difference is larger, while the temperature difference in laminar flow area is relatively small. Under the condition of the same initial temperature, the laminar flow and turbulent flow have obvious temperature difference after blowing. Two points corresponding to the laminar flow area and the turbulent flow area were selected respectively. By observing the temperature change with time, it was found that the heat loss in the turbulence area was greater than that in the laminar flow area, which also verified the above conclusion.

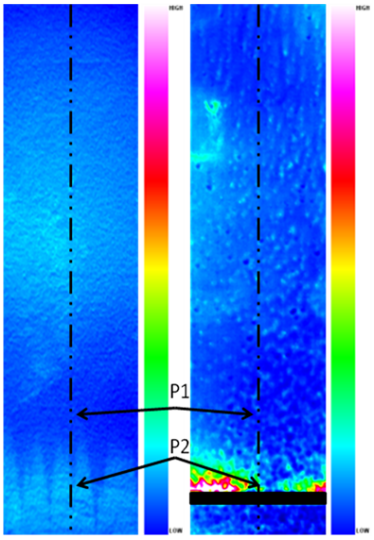

（1）Natural transition （2）Forced transition

Figure 36 Temperature distribution measured by TSP(Ma=0.7)

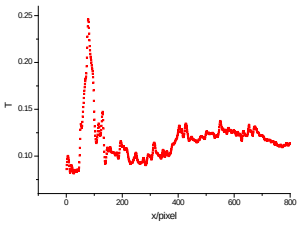

（1）Temperature distribution(Natural transition)

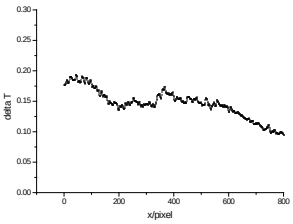

（2）Temperature distribution(Forced transition)

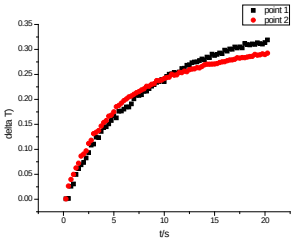

（3）Curve of temperature over time(Natural transition)

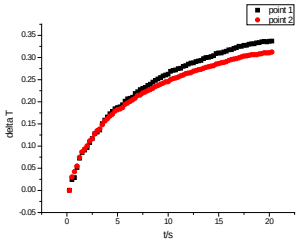

（4）Curve of temperature over time(Forced transition)

Figure 37 Transition results measured by TSP(Ma=0.7)

5 TOMOPIV test and results of airfoil

TOMOPIV is a 3d flow field visualization and measurement technology which reconstructs the spatial flow field through 2d images, including image preprocessing, 3d calibration, 3d particle reconstruction and 3d cross-correlation. The test was carried out in a sub-transonic and supersonic wind tunnel, the model was supercritical airfoil OAT15a and the test section was a double-layer structure with an outer circle and an inner square. The image acquisition system is composed of four CCD cameras, which are fixed on cradle heads with 6 degrees of freedom. Cradle heads and aluminum frame are connected, and the shooting Angle of camera can be adjusted by adjusting the cradle head. Four cameras were installed in settling chamber above the test section, with an overall square distribution. Particle images were recorded from different directions. Nd:YAG dual-pulse laser was placed in the side window of the test section. The output laser beam passes through one volume light source forming device to form a volume light beam with a certain thickness, and then passes through the adjustable diaphragm to form a volume light bean with regular boundary to illuminate the measuring area. The volume light source consists of laser beam expanding system and concave cylindrical lens. The laser beam expanding system consists of a plano-concave lens and a plano-convex lens to extend the diameter of the laser beam and reduce the divergence Angle of the laser beam. After beam expansion, the beam passes through a plano-concave cylindrical mirror, so

that the beam only expands in one direction to form a laser beam with elliptic section. After plano-concave cylindrical mirror, an adjustable aperture can be added to modify the boundary of the laser beam, so as to adjust the shape of the volume light beam needed for measurement.

Figure 38 Image acquisition system

Figure 39 Schematic diagram of volume light source

Figure 40 Arrangement of volume light source

The three-dimensional flow field behind the trailing edge of the airfoil was measured, and the inlet Mach number was 0.6 and 0.7 respectively, and the Angle of attack was 0 degrees. It can be seen from the Mach number distribution of the flow field under Ma=0.6 and 0.7 that the Mach number of the flow field increases after attaching the micro riblets film, indicating that the micro riblets film has a certain effect of drag reduction.

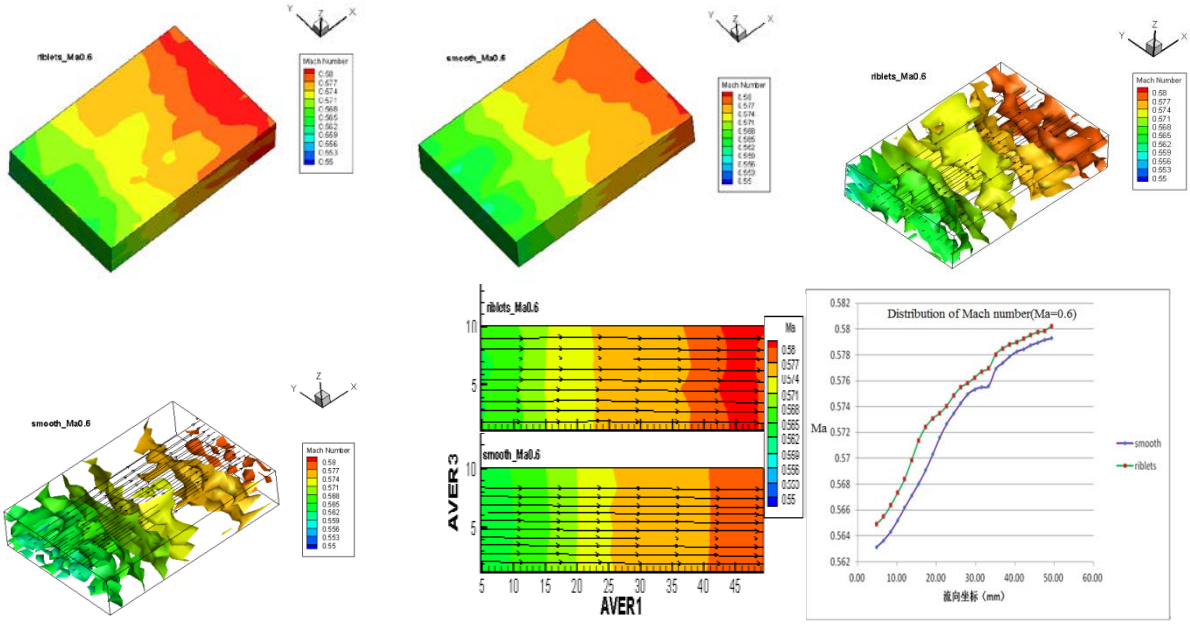

Figure 41 Distribution of the Mach number of smooth film and micro riblets flow field(Ma=0.6)

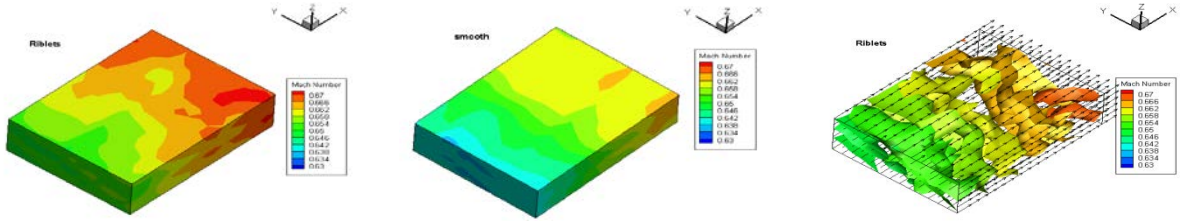

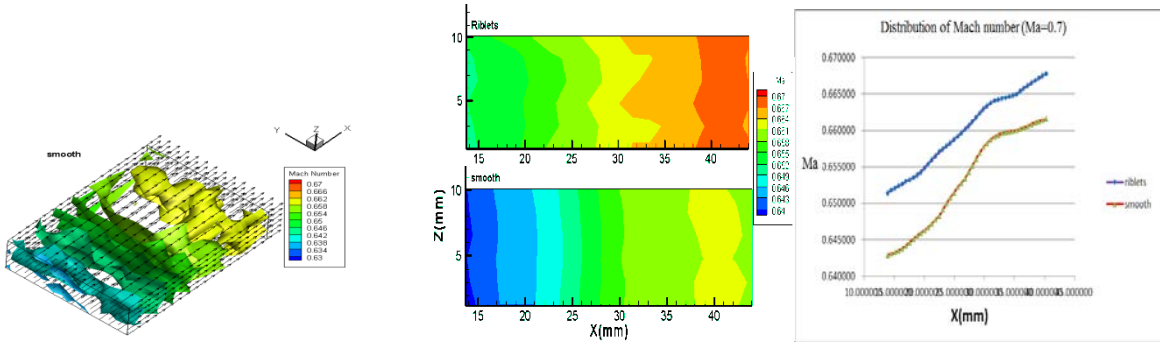

Figure 42 Distribution of the Mach number of smooth film and micro riblets flow field(Ma=0.7)

6 fluorescence oil film test and results of plate

The flat plate model is used in the oil film friction test, which can more directly and effectively measure the influence of the presence of micro riblets film on the skin friction. In order to better compare the difference between smooth film and micro riblets film, oil film was coated on the model behind film. Smooth film and micro riblets film were respectively pasted on the left and right sides of the symmetry line of the model, or different micro riblets films were pasted, and the drag reduction effect of rib film was verified under the same flow condition. The experiment measured the two comparative layouts under Mach 0.6 flow condition, namely (1) smooth film and micro riblets film 1#, (2) micro riblets film 1# and micro riblets film 2#. The oil film friction test light source of the flat plate model is a 600 watt xenon lamp ultraviolet light source. Pmx-200z silicon oil was used in the experiment, and the viscosity (kinematic viscosity coefficient) was 12500CS. The fluorescent substances dissolved in the silicon oil could emit orange light under ultraviolet lamp.

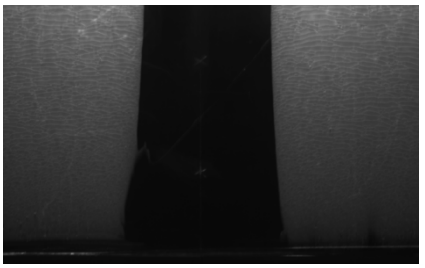

（a）Oil film comparison (Smooth film (left) and micro riblets film 1# (right))

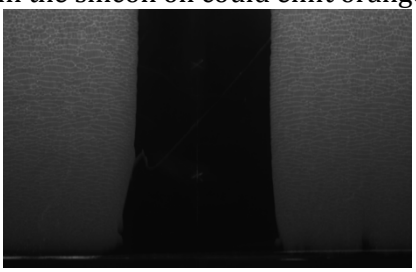

（b）Oil film comparison(micro riblets film 2# (left) and micro riblets film 1# (right))

Figure 43 Oil film comparison diagram of different layouts

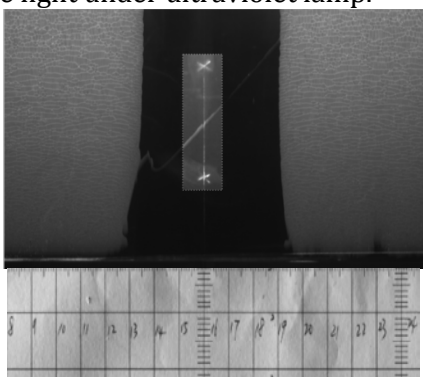

Figure 44 Highlighted mark graphs

Figure 43 shows the oil film comparison diagram of different layouts. The flow direction is from bottom to top, and the lower bright band boundary is the tail of the smooth film or micro riblets film. The image has been processed with grayscale stretching for better visualization. It can be seen that the oil film spreads well under the shear stress of incoming flow.

In the test, the image has certain jitter at different moments due to the action of airflow. For this reason, marked graphs are depicted on the symmetric line in the middle of the model, marked points are identified through image post-processing, and images at different moments are shifted by mark points to eliminate errors caused by image jitter.

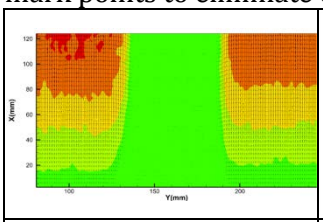

Figure 45 Relative skin

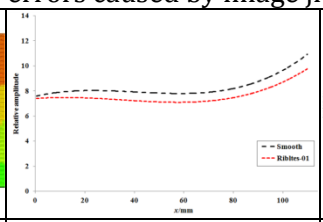

Figure 46 Comparison of

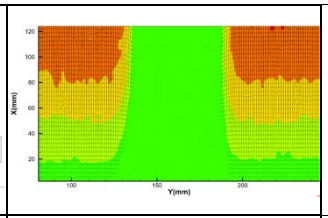

Figure 47 Relative skin

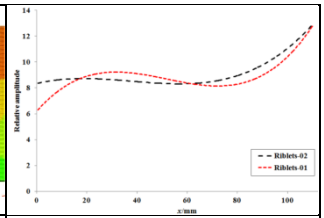

Figure 48 Comparison of

friction amplitude distribution (Smooth film (left) and micro riblets film 1# (right))	relative skin friction amplitude after spanwise average (Smooth film (left) and micro riblets film 1# (right))	friction amplitude distribution (micro riblets film 2# (left) and micro riblets film 1# (right))	relative skin friction amplitude after spanwise average (micro riblets film 2# (left) and micro riblets film 1# (right))

Figure 45 is relative skin friction amplitude distribution (Smooth film (left) and micro riblets film 1# (right)). Figure 46 is Comparison of relative friction amplitude distribution after spanwise average (Smooth film (left) and micro riblets film 1# (right)). Figure 47 is Relative skin friction amplitude distribution (micro riblets film 2# (left) and micro riblets film 1# (right)). Figure 48 is Comparison of relative friction amplitude distribution after spanwise average (micro riblets film 2# (left) and micro riblets film 1# (right)). It can be seen that, compared with smooth film, micro riblets film has obvious drag reduction effect, while skin friction distribution of the rear surface of micro riblets film 2# and micro riblets film 1# is relatively close, which also indicates that the two kinds of micro riblets films have little difference in drag reduction effect.

In order to quantify the comparison of the magnitude of friction resistance, integral average is conducted for the friction amplitude values in the statistical area, and the integral difference obtained can be regarded as the magnitude value of friction resistance reduction. According to this, the calculation formula of the percentage of skin friction reduction is:

$$\varepsilon = \frac{S_{\text{Smooth}} - S_{\text{Riblet}}}{S_{\text{Smooth}}} \times 100\% \tag{2}$$

Table 3 Drag reduction percentage of different film contrast

	riblets film 1# vs smooth film	riblets film 1# vs riblets film 2#
Drag reduction percentage	8.36%	2.3%

In terms of percentage of drag reduction, both 1# and 2# micro riblets film have drag reduction effect. It seems that 1# micro riblets film has better drag reduction effect than 2# micro riblets film.

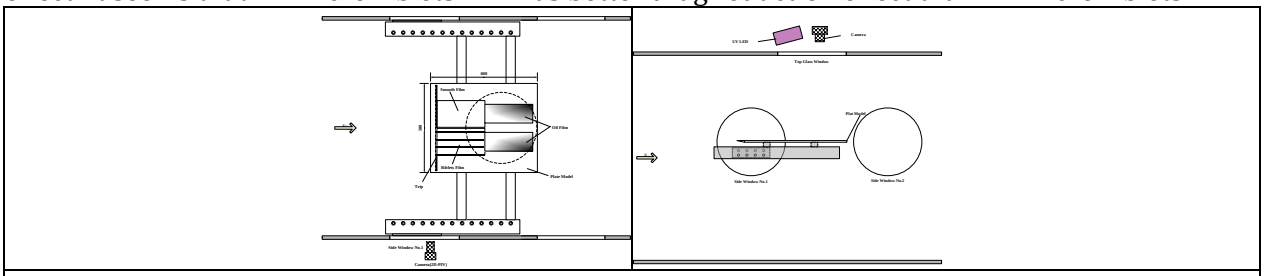

Figure 49 Layout of PIV test

7 Conclusion

In this paper, a transonic wind tunnel test is carried out to verify the drag reduction mechanism of micro riblets of supercritical airfoil model. PSP/TSP was used to determine the flow pattern on the surface of aerofoil. PIV and TOMOPIV were used to verify the drag reduction effect of micro riblets. Similarly, PIV and fluorescent oil film were carried out for the flat model to verify the drag reduction effect of micro riblets. The experimental results of PIV showed that the use of micro riblets film can improve the velocity (Mach number) in the boundary layer and reduce the fluctuation velocity intensity in the near-wall region. The experimental results of PSP/TSP showed that the surface pressure distribution was in accord with the theory, and the gap flow had little influence, and the airfoil surface was developed into turbulence after manual forced transition. The experimental results of TOMOPIV showed that the micro riblets can improve the flow velocity (Mach number) of the three-dimensional flow field behind the trailing edge of the airfoil. The experimental results of fluorescent oil film showed that the micro riblets film can reduce the surface friction and has the effect of reducing the friction.

All these experimental results show that under the condition of turbulence, micro riblets film changed flow state in near wall region, reduce fluctuation velocity in near wall region, reduce

energy loss caused by turbulence, thus improve flow velocity (Mach) in boundary layer and flow velocity (Mach) in three dimensional flow field behind trailing edge of airfoil, reduce skin friction, realize the drag reduction effect.

Acknowledgements

This work was sponsored by the national key basic research project (2014CB744805, 2014CB744801)

References

[1] Walsh M J. Riblets: viscous drag reduction in boundary layers [R]. NASA Technical Report,Virginia, 1990.

[2] Wang J J ,Lan S L, Lian Q X. Effect of the riblets surface on the boundary layer development[J]. Chinese Journal of Aeronautics, 1996, 9 (4) : 257 - 260.

[3] LAN S L, WANG J J. Experimental Comparison between the Turbulent Boundary Layers for Corrugated and Flat Surfaces[J]. JOURNAL OF EXPERIMENTAL MECHANICS, 1998, 13 (1) : 28 - 33(in Chinese).

[4] WANG J J, LAN S L, CHEN G. Experimental Study on the Turbulent Boundary Layer Flow over Riblets Surface[J]. ACTA MECHANICA SINICA, 2000, 32 (5): 621 - 626(in Chinese).

[5] Choi K S. Effects of longitudinal pressure gradients on turbulent drag reduction with riblets turbulence control by passive means[M]. Norwell, Kluwer academicMA, 1992.

[6] Bacher E V, Smith C R. A combined visualization anemometry study of the turbulent drag reducing mechanisms of triangular micro2 groove surface modifications [R]. American: AIAA, 1985.

[7] Pulles C J A, Prasad K K, Nieuwstadt F TM. Turbulence measurements over longitudinal micro2 grooved surfaces[J]. App lied Scientific Research, 1989, 46 (2) : 197.

[8] Choi K S. Nearwall structure of turbulent boundary layer with riblets[J]. Journal of Fluid Mechanics, 1989, 208(4) : 417 - 458.

[9] Tang Y P,Clark D G. On near2all turbulence2generating events in a tubulent boundary layer on a riblet surface [J]. App lied Scientific Research, 1993, 50: 215 - 232.

[10] WANG J J, CHEN G. Experimental Studies on the Near Wall Turbulent Coherent Structures over Riblets Surfaces[J]. Acta Aeronautica et Astronautica Sinica, 2001, 22 (5) : 400 - 405 (in Chinese).

[11] S.-J. Lee, Y.-G. Jang. Control of flow around a NACA 0012 airfoil with a micro-riblet film[J]. Journal of Fluids and Structures 20 (2005) 659–672.

[12] Hefner J N, Bushnel D M,Walsh M J. Research on non-planarwall geometries for turbulence control and skin-friction reduction[A]. 8th U. S. 2FRG DEA2Meeting, Viscous and interacting flow field effects[C] , Gottingen, 1983.

[13] WalshM J. Riblets as a viscous drag reduction technique [J]. A IAA Journal, 1983, 21 (4) : 485 - 486.

[14] Walsh M J. Turbulent boundary layer drag reduction using riblets[R]. American: AIAA, 1982.

[15] Walsh M J. Lindemann A M. Optimization and application of riblets for turbulent drag reduction[R]. American: AIAA, 1984.

[16] Leonardo P. Chamorro, R.E.A. Arndt, F. Sotiropoulos. Drag reduction of large wind turbine blades through riblets: Evaluation of riblet geometry and application strategies. Renewable Energy 50 (2013) 1095-1105.

[17] Lazos B S, Wilkinson S P. Turbulent viscous drag reduction with thin-element-riblets[J]. A IAA Journal, 1988, 26 (4) : 496 – 498.

[18] Choi H, Moin P, Kim J. Direct numerical simulation of turbulent flow over riblets [J]. Journal of fluid mechanics, 1993, 255: 503 - 539.